

Article

Microstructures and Wear Resistance of Boron-Chromium Duplex-Alloyed Coatings Prepared by a Two-Step Pack Cementation Process

Jianjun Hu ^{1,2}, Jing Zeng ¹, Yan Yang ³, Xian Yang ¹, Hui Li ^{1,*} and Ning Guo ^{4,*} 

¹ College of Material Science and Engineering, Chongqing University of Technology, Chongqing 400054, China

² Chongqing Municipal Key Laboratory of Institutions of Higher Education for Mould Technology, Chongqing University of Technology, Chongqing 400054, China

³ College of Mechanical Engineering, Chongqing University of Technology, Chongqing 400054, China

⁴ School of Materials and Energy, Southwest University, Chongqing 400715, China

* Correspondence: lihui@cqut.edu.cn (H.L.); guoning_1000@163.com or whc34@swu.edu.cn (N.G.); Tel.: +86-23-6256-3178 (H.L.); +86-23-6825-3204 (N.G.)

Received: 1 August 2019; Accepted: 21 August 2019; Published: 21 August 2019



Abstract: In this study, a two-step pack cementation process (preboronizing and then chromizing) was employed to prepare the B-Cr duplex-alloyed coating on the steel. After the first step of preboronizing (PB sample), box-type furnace chromizing (BC-1 sample) and induction heating chromizing (BC-2 sample) were carried out, respectively. The phases and microstructure of the coatings were characterized by X-ray diffraction (XRD), backscattering electron imaging (BSEI), and energy dispersive spectroscopy (EDS). The results reveal that the heating mode of the second step of chromizing has a significant effect on the phase composition and microstructure of the B-Cr coating. The efficiency of induction heating is higher than that of the box furnace heating, resulting in a thicker, denser, flatter surface, and B-Cr coating with fully reacted B and Cr elements. The wear and corrosion resistance of the steel is found to be significantly improved by the formation of effective B-Cr coating. The formation mechanisms and properties of the two duplex-alloyed coatings are investigated and discussed.

Keywords: boronizing; chromizing; pack cementation; duplex-alloyed coating; wear resistance

1. Introduction

For many mechanical parts (e.g., transmission shafts, gears, and dies), good wear resistance, corrosion resistance, and high-temperature oxidation resistance must be possessed in order to meet the growing demand in harsh environments, which are characterized by high speed, heavy load, high temperature, a corrosive environment, and so on [1–4]. Many studies [3–5] have shown that surface modification techniques are highly effective methods which can improve the service performances of the parts. Exploring novel coatings to improve the surface performances of metals and alloys has always been a great challenge in the field of materials science [6].

Nowadays, diffusion coatings on gear materials via carburizing, nitriding, carbonitriding, boronizing, and chromizing to improve the wear resistance of carbon steels has been widely reported [7–10]. In addition to improvement on the hardness and wear resistance, boronizing and chromizing treatment can also improve the corrosion resistance and high-temperature oxidation resistance of carbon steels. It has been reported that the boronizing coating with a high hardness of 1200–2000 HV has good wear resistance [11–14], as a result of the formation of hard phases of the types $M_{23}(C,B)_6$, $M_3(C,B)$, M_2B , and M_3B_2 [15]. However, the application of boronized coating in many fields (especially boronizing on the surface of carbon steels) are limited by the brittleness and poor cohesion [11]. Recently,

Hu et al. [1,4] reported that a carbon-poor zone between Cr-coating and substrate was noticed during high-temperature chromizing. It is well-known that a carbon-poor zone is harmful to the performances of parts, due to its low hardness.

Thermo-reactive diffusion and deposition (TRD) is a thermo-chemical coating treatment method [6,16–18]. Pack cementation, one of the TRD treatment methods, is widely applied to metals or alloys to improve their surface performances [19], which is low-cost, effective, and easy to operate. Pack boronizing and chromizing have been studied by many researchers for a long time. Petrova et al. [20] claimed that a coating with a thickness of 75–80 μm on the surface of low-carbon steel could be obtained by pack boronizing in a furnace at 850 $^{\circ}\text{C}$ for 4 h. The thick boronizing layer is attributed to the small-size boron atoms which can easily diffuse into steels [20–22]. However, some of the literature show that only a very thin coating can be prepared by conventional pack chromizing with a long processing time (more than 10 h) [4,23].

Considering the advantages and disadvantages of boronizing and chromizing, chromium-boron composite coatings [12,24] have been prepared by a few researchers. The results showed that the properties of composite coatings were better than single coatings. In addition, it was found that the coatings treated via boronizing followed by chromizing resulted in more excellent performances than chromizing followed by boronizing [24]. However, there was still a long processing time, which indicates that the conventional preparation methods of composite coatings are uneconomical.

In this study, in order to shorten the processing time and obtain thicker composite coatings on the commercial AISI 5140 steel resulting in better performance, a new preparation process for a boron-chromium composite coating has been explored. In the authors' research group, induction heating pack chromizing (IC) has been investigated deeply, and it has been demonstrated that the thicker coating can be obtained by IC treatment in a short time [1,4]. Thus, in the present work, after preboronizing (PB), box-type furnace heating pack chromizing (BC-1) and induction heating pack chromizing (BC-2) were carried out on the AISI 5140 steels. Then, the microstructures, formation mechanisms, and properties of the two composite coatings were investigated, and properties including microhardness, wear, and corrosion resistance were studied and compared.

2. Materials and Methods

2.1. Sample Preparation

Commercial AISI 5140 steel (Fe-0.40C-0.80Cr-0.27Mn-0.23Si-0.03Ni, in wt.%) was selected as the starting material, and cut into cuboid samples with a gauge dimension of 25 mm \times 20 mm \times 6 mm. Before pack cementation, complete austenitizing (860 $^{\circ}\text{C}$ for 1 h) and water quenching treatments were carried out on the cuboid samples, followed by a high-temperature tempering treatment (580 $^{\circ}\text{C}$ for 1 h). The samples were then mechanically polished and ultrasonically cleaned in alcohol.

A two-step pack cementation process was employed here to prepare the B-Cr duplex-alloyed coating on the steel, as shown in Table 1. Powder compositions for the two-step pack cementation process were as follows: 50 wt.% ferrobore (containing 20 wt.% B and 80 wt.% Fe) as feedstock, 5 wt.% KBF_4 as the activator, 5 wt.% La_2O_3 as the modifier, and 40 wt.% Al_2O_3 as the inert filler for the first step of boronizing, and 45 wt.% Cr as feedstock, 5 wt.% NH_4Cl as the activator, 5 wt.% La_2O_3 as the modifier, and 45 wt.% Al_2O_3 as the inert filler for the second step of chromizing. All the above powders, having a particle size less than 75 μm in diameter, were mixed by a blender for 1 h. The first packed powders and steel specimens were put in a ceramic crucible (30 mL), and then heated to 950 $^{\circ}\text{C}$ and held at that temperature for 3 h in a box-type furnace. Subsequently, the boronized samples were immersed in the second pack mixtures and heated to 1000 $^{\circ}\text{C}$ for 1 h. In the second step, both box-type furnace heating and induction heating were employed for chromizing to investigate the effect of heating and cooling rates on the microstructure and properties of the B-Cr coating. After the pack cementations, all the samples were naturally cooled to room temperature. In addition, prior to the second step, all the preboronized samples were cleaned.

Table 1. Coating histories of various samples in this study.

Sample	Coating History	
	Step 1 (950 °C for 3 h)	Step 2 (1000 °C for 1 h)
PB	Boronizing	–
BC-1	Boronizing	Chromizing (box-type furnace heating)
BC-2	Boronizing	Chromizing (induction heating)

2.2. Characterization and Performance Test Methods

Cross-sectional microstructures and morphologies of tempered and coated samples were observed using secondary electron imaging (SEI) and backscattering electron imaging (BSEI) detectors installed in a field emission gun scanning electron microscope (FEGSEM, Zeiss Sigma HD, Zeiss, Dresden, Germany). Energy dispersive spectroscopy (EDS, AZtech Max2, Oxford Instruments, London, UK) equipped in the FEGSEM was employed to characterize the distribution of various elements. An X-ray diffractometer (XRD, Empyrean Series 2, PANalytical, Almelo, The Netherlands) with a Cu K α radiation was used to identify the phase components of the coatings, with a step size of 0.013° and angle range of 20° to 90°. Prior to characterization, the samples were ground and subsequently electropolished with an electrolyte of 10% perchloric acid and 90% alcohol at about –30 °C for 60 s.

Vickers hardness from surface to substrate was measured on a microhardness tester (HVS-1000Z, Shanghai CSOIF Co., Ltd., Shanghai, China), with a load of 2 N and a dwelling time of 10 s. Friction and wear tests were carried out on a reciprocating tribometer (HSR-2M), using steel balls (AISI 52100, Fe-1.0C-1.5Cr-0.30Mn-0.25Si-0.1Mo, in wt.%) with a diameter of 6 mm as friction pairs. The parameters were presented as follows: load 15 N, duration time 30 min, frequency 2 Hz, and wear scar length 10 mm. The potentiodynamic polarization curves tested in a 3.5% NaCl solution using a Gamry instrument (Reference 3000, Warminster, PA, USA) were used to evaluate the corrosion behavior of the tempered and coated samples. The dynamic potential range was –1 to 3.5 V, and the scanning speed was 2 mV/s.

3. Results and Discussion

3.1. Phases Analysis and Microstructures Characteristics

After quenching and tempering, typical tempered sorbite morphology could be observed, as shown in Figure 1. It can be seen that the rod-like and spherical carbide particles are uniformly dispersed in the ferrite grains. It has been pointed out that the uniform distribution of carbides facilitates the formation of uniform coatings [4].

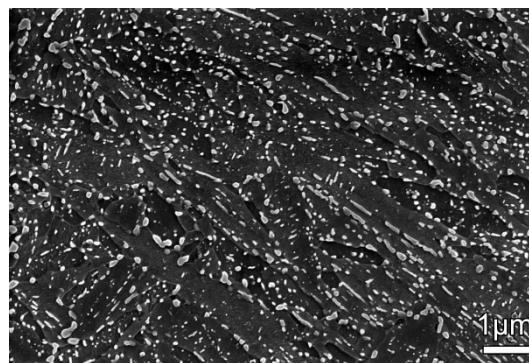


Figure 1. Secondary electron imaging (SEI) image showing the microstructure of the starting material.

Figure 2 shows the XRD patterns of the various samples before and after the coating treatments. All kinds of phases were determined by using International Diffraction Data Center (ICDD) database,

with the 2004 version of the powder diffraction file (PDF) database. Before coating treatment, the ferrite with a body-centered cubic (BCC) structure can clearly be seen on the XRD pattern of the substrate. After the first step of boronizing, in the PB sample, there is no ferrite phase, and only the Fe₂B phase can be detected. It is indicated that a Fe₂B coating has formed on the substrate, and the Fe₂B coating has a certain thickness to completely shield the ferrite diffraction information of the substrate. According to the literature, the formation of single-phase Fe₂B or two-phase Fe₂B and FeB depends on the boron potential in the boronizing media, process time, and temperature [25]. After the second step of chromizing, the Fe₂B and Cr-rich phase (containing Cr₂B, CrC, and Cr_{0.1}Fe_{1.9}) are observed in the BC-1 sample, while pure Cr, chromium boride Cr₂B, and chromium carbides Cr_xC_y (Cr₂₃C₆ and Cr₇C₃), τ-phase Fe₂₃(C,B)₆ are detected in the BC-2 sample. It can be seen that at the same processing temperature and time, the difference in heating mode also affects the phase composition of the coatings. For the box furnace heating, the chromization rate is very low, so after the chromizing treatment, a large amount of Fe₂B is retained in the BC-1 sample. On the contrary, for the induction heating, the chromizing rate is very fast, and the Fe₂B (formed during the preboronizing) and Cr elements (from chromizing) and/or C atoms (from the substrate) react to form chromium boride, and disappear in the coating of the BC-2 sample. This is because the diffusion velocity of atoms is remarkably accelerated during the induction heating [4]. According to the literature, it needs to be demonstrated that the τ-phase Fe₂₃(C,B)₆ is formed in a lower B concentration with a temperature close to the austenite-ferrite transition temperature (700–1000 °C) [26]. In this study, the lower B concentration in the coating was caused by decomposition of Fe₂B and the migration of boron atoms from the interior to exterior.

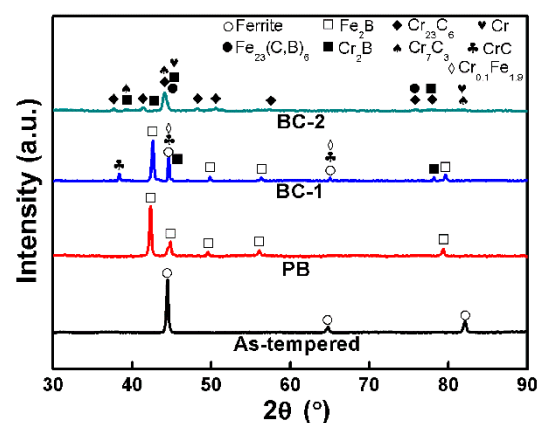


Figure 2. X-ray diffraction (XRD) patterns of the AISI 5140 steel after PB, BC-1, and BC-2 treatments.

3.2. Microstructures after Preboronizing

Figure 3 presents the cross-sectional microstructure of the PB sample. In Figure 3a, it can clearly be seen that the outermost layer of the coating consists of columnar grains, with the length direction perpendicular to the surface of the coating. The EDS results show that these columnar grains contain more B and Fe elements, as shown in Figure 3b. Combined with EDS and XRD data, the columnar grains are considered to be Fe₂B. The presence of columnar Fe₂B grains results in the coating having a rough surface, thus resulting in a typical saw-toothed B-coating. The mean value of the total boride coating can be calculated by using the formula [27]:

$$d = \frac{\frac{\sum_{i=1}^n a_i}{n} + \frac{\sum_{i=1}^n b_i}{n}}{2} \quad (1)$$

where d is the average thickness of the coating, n is the number of selected short or long columnar grains, a_i and b_i are the length of each short and long columnar grain (respectively marked as a_1, a_2, a_3 , etc., and b_1, b_2, b_3 , etc., in Figure 3a). In this study, the average thickness of the B-coating is determined

as about 69 μm . Figure 3c shows the interface between the coating and substrate. It can be seen that the interface is irregularly curved, and the B-coating and substrate penetrate each other, indicating that the interface has a good bonding force. The high-magnification image shows that the substrate has a typical hypoeutectoid steel structure consisting of a mixture of ferrite grains and pearlite colonies, as shown in Figure 3d.

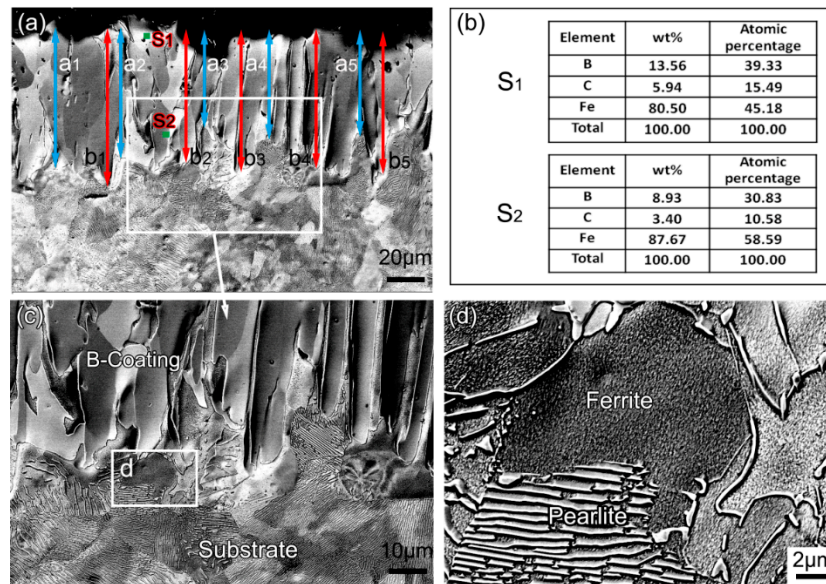


Figure 3. Sectional microstructure of the preboronizing (PB) sample: (a) backscattering electron imaging (BSEI) image of the coating; (b) energy dispersive spectroscopy (EDS) patterns of two selected points (S₁ and S₂) in (a); (c,d) high-magnification BSEI images corresponding to the white boxes.

3.3. Microstructures after Chromizing

Figure 4 shows the microstructure and elemental distribution of the BC-1 after the second step of chromizing. After the box furnace heating chromizing, the columnar Fe_2B grains can still be seen, as shown in Figure 4a,c. The coating thickness is measured to be about 70 μm , which is similar to the thickness of the coating after preboronizing. The high-magnification micrograph (Figure 4b) and EDS indicate that a thin layer of Cr-rich is deposited on the outer layer of the columnar Fe_2B grains. According to the XRD results (see Figure 2), it is considered that the Cr-rich layer is mainly composed of Cr_2B , CrC , and $\text{Cr}_{0.1}\text{Fe}_{1.9}$. However, the Cr-rich layer contains a large number of pores and cracks (see Figure 4b), indicating poor properties. It is reported that the existence of pores is attributed to the difference in diffusion rates between various elements [24], and the formation of cracks is mainly caused by stress concentration caused by different coefficients of thermal expansion of different phases in the coating [2,28]. In addition, some granular borides (see white arrows in Figure 4c) can also be observed near the interface between the coating and the substrate. Owing to a lower carbon and boron potential on the surface, a large amount of boron and carbon atoms migrate from the inside (the B-coating after preboronizing treatment) to the coating surface during the heating and holding process of chromization, resulting in the formation of such granular borides. It can be concluded that after the box furnace heating at 1000 $^\circ\text{C}$ for 1 h, the Cr element is not completely penetrated into the B-coating, and no effective B-Cr duplex-alloyed coatings is formed on the steel substrate.

Microstructure and elemental distribution of the BC-2 sample are depicted in Figure 5. Figure 5a reveals a thick, dense, and flat coating with a thickness of 180–190 μm , which is about 2.7 times the thickness of the PB or BC-1 coating. Moreover, no significant pores and cracks can be observed in the coating. As shown in Figure 5c, the EDS line scanning results show that the content of Cr in the coating is significantly higher than that of Fe, indicating that the Cr element has penetrated into the

original B-coating formed in the first step of preboronizing. That is, for the second step of chromizing, induction heating chromizing is much better than box furnace heating.

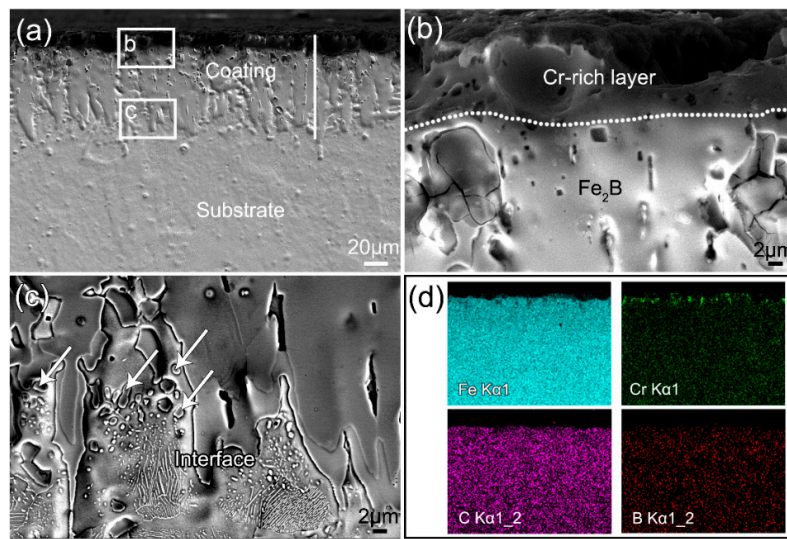


Figure 4. Microstructure and elements distribution after the BC-1 treatment: (a) sectional SEI view of the coating; (b,c) high-magnification SEI and BSEI images corresponding to the white boxes; (d) the EDS mapping corresponds to the entire area in (a).

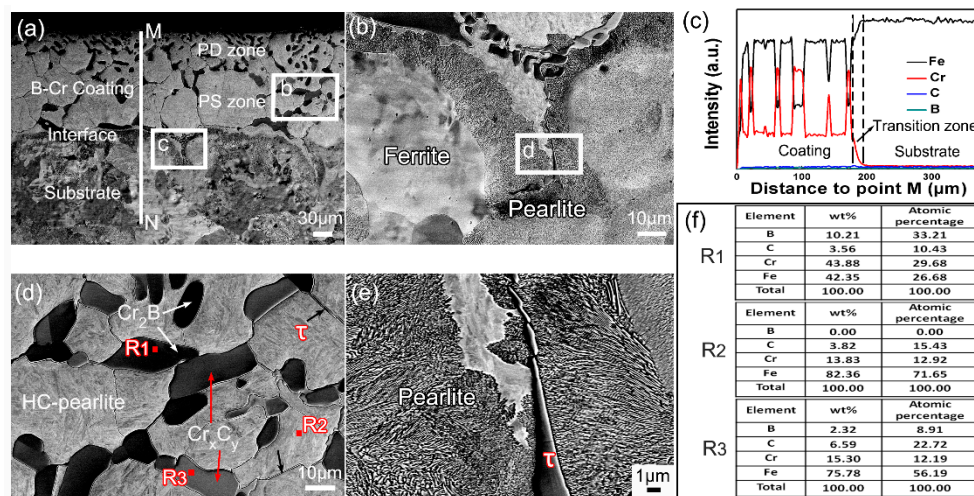


Figure 5. Microstructure and elements distribution after the BC-2 treatment: (a) BSEI image of the cross-section; (b,d,e) high-magnification BSEI image corresponding to the white boxes; (c) EDS line scanning; (f) EDS point analysis of R1, R2, and R3 in (d).

From Figure 5a, it can be seen that the columnar Fe_2B grains formed during preboronizing disappeared and were replaced by equiaxed grains with an average grain size of about $65 \mu m$. The high-magnification micrograph (see R2 in Figure 5d) and EDS results (see R2 in Figure 5f) confirm that the equiaxed grains are pearlite, with high Cr content (HC-pearlite). Such HC-pearlite morphology has also been detected in coatings of the thermal diffusion-chromized AISI 5140 steel. Interestingly, a large amount of second-phase particles (see the dark area in Figure 5a) can be detected in the coating. A large change in Cr intensity along the EDS line (see Figure 5c) also indicates that the coating consists of different phases. Obviously, the second phase is densely distributed (PD region) in the region near the outer surface of the coating, and sparsely distributed (PS region) in the region near the substrate. The gradient distribution of the second phase can result in a gradient of properties. As shown in Figure 5d, three kinds of second phases included can be distinguished from the enlarged micrograph:

a gray block (red arrows), black block (white arrows), and gray band (black arrows). According to the EDS data analysis of points R1 and R3 (Figure 5f), it is known that the B and Cr contents of R1 are higher than R2. Additionally, since the lighter elements reflect less backscattered electrons [29], the Cr_2B phase, having a lower average atomic number than Cr_xC_y , is darker in the BSEI image. Thus, it can be inferred that the dark block is composed of the Cr_2B phase, while the gray blocks consist of Cr_xC_y . The second phase of the gray band (see Figure 5d) is always distributed at the grain boundary of HC-pearlite, or at the phase boundary of HC-pearlite and Cr_2B (or Cr_xC_y). It is too thin to accurately determine their chemical composition by EDS technology in this study, as shown in Figure 5d. It has been reported that the nucleation and precipitation of $\text{Fe}_{23}(\text{C},\text{B})_6$ (τ -phase) mainly occur at the grain or subgrain boundaries [30]. It is considered that the gray band shape corresponds to τ . In addition, the substrate still presents a typical hypoeutectoid steel structure, consisting of ferrite grains and pearlite colonies, as shown in Figure 5b,e.

3.4. Formation Mechanism of the B-Cr Duplex-Alloyed Coatings

The formation mechanism of the B-Cr coating of the BC-1 and BC-2 samples is depicted in Figure 6. The formation mechanism of the B-coating in the process of boronizing has been widely reported [31], so only the evolution mechanism of the coating during the second step of chromizing is discussed here. Figure 6a displays the schematic microstructure of the PB sample after preboronizing. Whether it is box furnace heating or induction heating, as shown in Figure 6b, austenitization involving decomposition of cementites and redistribution of C atoms takes place in the preboronized sample at the beginning of chromizing ($\sim 900^\circ\text{C}$). According to the Fe-B binary phase diagram [15,26], the Fe_2B and $\gamma\text{-Fe}$ (face-centered cubic structured) coexist at the temperature of austenitization. When the temperature rises to the chromizing temperature (1000°C), the Fe_2B starts to decompose, but due to the kinetics, it takes a certain time to completely decompose. For box-type furnace heating, the Fe_2B (B-coating) does not completely decompose during the one-hour heating. Some Fe_2B grains are retained (see Figure 6c1), while for induction heating, Fe_2B completely decomposes and diffuses (see Figure 6c2). That is to say, the efficiency of induction heating is higher than that of the box furnace heating, and this phenomenon has been reported in the literature [4]. Meanwhile, the C, B, Fe, and Cr atoms begin to diffuse due to their high chemical potentials. Owing to the low atomic diffusion rate of box-type furnace heating, a thin diffusion layer of chromium (Cr-rich layer) is formed on the Fe_2B after cooling in the BC-1 sample (see Figure 6d1). For the induction heating, after cooling, the original B-coating completely decomposes, and the elements re-diffuse and react with other elements to form chromium compounds of Cr_2B and Cr_xC_y in the BC-2 sample, as shown in Figure 6d2. In addition, the τ -phase precipitates at the grain boundaries and phase boundaries during the cooling process, as shown in Figure 6d2.

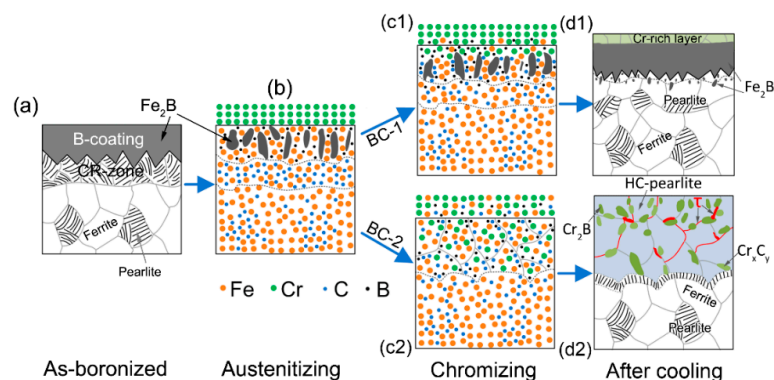


Figure 6. Sketch maps showing atomic diffusion process and microstructure evolution during chromizing after preboronizing: (a) before chromizing; (b) austenitizing at the beginning of chromizing; (c1,c2) during chromizing; (d1,d2) final equilibrium microstructures after cooling to room temperature.

3.5. Properties

3.5.1. Microhardness

Figure 7 exhibits the hardness distribution along the depth direction of various samples. As can be seen, the hardness of the three kinds of samples decreases from coating to substrate, and tends to keep stable at the substrate. For the PB sample, the coating has the highest hardness (1606 HV) at the subsurface of the coating, due to the existence of the columnar grained Fe_2B . Fe_2B is a hard boride with higher hardness than Cr_2B and Cr_xC_y [15,32]. However, due to defects such as voids and cracks (see Figure 3a) in the coating of the PB sample, the overall hardness of the coating is not uniform, and in some places, the hardness is only 923 HV. After chromizing, the Fe_2B is partially (in the BC-1 sample) or completely (in the BC-2 sample) dissolved, resulting in a significant decrease in hardness of the coating. For the BC-1 sample, the surface hardness of the coating is about 886 HV, while for the BC-2 sample, it is about 858 HV. Although the hardness of the coating after chrome plating is significantly reduced, the thickness of the coating is significantly increased. It is worth noting that there is no significant carbon-poor zone in the BC-1 or BC-2 samples. It has been widely reported that for the single-step chromized steels, a carbon-poor zone is always present between the coating and the substrate, resulting in a lower hardness than the substrate and coating [1–4,33]. For thermal chromizing treatment, the subsurface decarburization is a chronic disease. Fortunately, the two-step pack cementation process can effectively solve the problem of subsurface decarburization. It can be speculated that prior to the chromizing treatment, precarburing or prenitriding can also avoid the occurrence of subsurface decarburization.

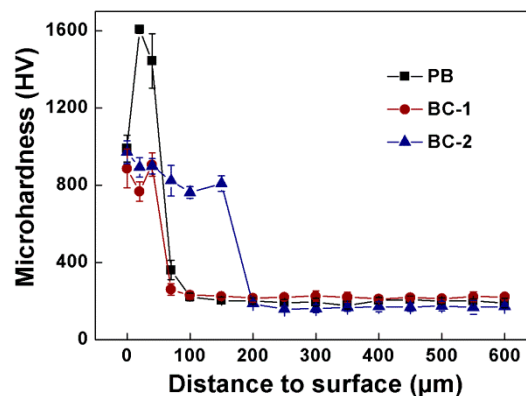


Figure 7. Microhardness plotted as a function of distance to the coating surface of various samples.

3.5.2. Wear Resistance

Studies have shown that some composite coatings have outstanding wear resistance [34,35]. Figure 8 shows the wear morphologies of various samples. In Figure 8a, the tempered sample has a wear track width of about 676 µm in width, and there are a lot of wear marks and pits on the surface. The wear track widths of the PB, BC-1, and BC-2 samples are about 744, 708, and 584 µm, respectively (see Figure 8b–d). It should be noted that the friction pairs (steel balls) have a hardness of 720–760 HV in this study. For the PB sample, the coating is very hard, resulting in severe wear of the friction pairs during the wear test, so the measured wear track width may be wider than the true width. The BC-2 sample has the lowest wear track width, indicating good wear resistance. Figure 9a displays the mass loss of various samples in wear testing. There is no doubt that the mass loss of the tempered sample is the largest, due to severe exfoliation. Owing to the surface irregularities and porosity (see Figure 3a), the mass loss of the PB sample is greater than the mass loss of the BC-1 and BC-2 samples. In addition, the mass loss of the BC-1 sample is greater than that of the BC-2 sample. These further confirm that the BC-2 coating has good wear resistance.

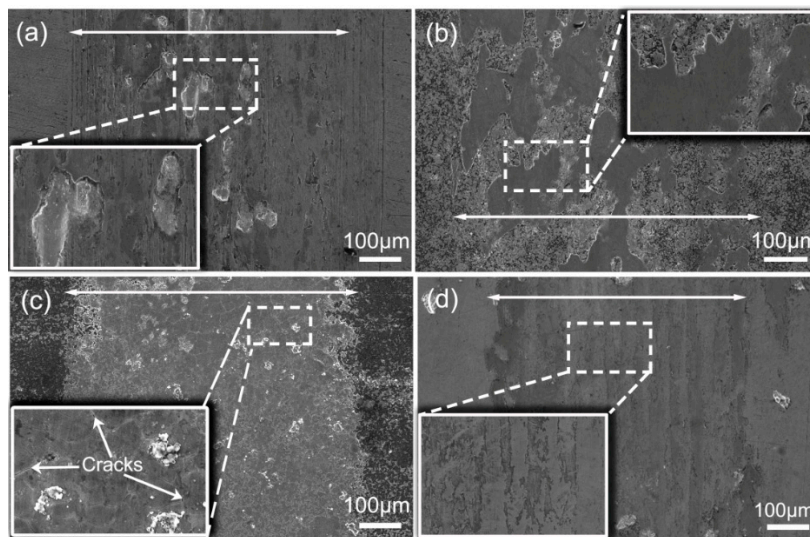


Figure 8. Wear morphologies of various samples: (a) starting material; (b) PB; (c) BC-1; (d) BC-2.

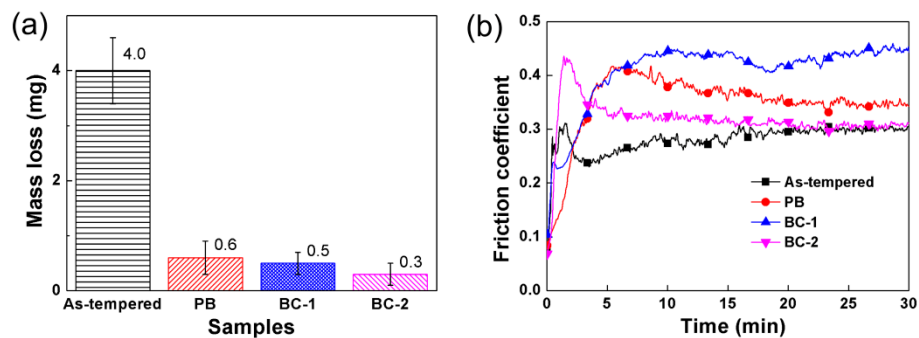


Figure 9. Mass loss and friction coefficient plotted as a function of sliding friction time for various samples.

The friction coefficients plotted as a function of friction time for the various samples is presented in Figure 9b. Generally, the smaller the coefficient of friction is, the better the wear resistance of the material. However, the tempered material is mechanically polished, while the coated sample is not mechanically polished before the abrasion test. That is, the surface roughness of the sample varies greatly prior to the wear test. It is well-known that the roughness of the sample surface has a large effect on the wear behavior and the friction coefficient, especially in the early stage of wear. Therefore, the tempered sample has the lowest friction coefficient in the initial stage of wear, owing to the fact that the surface of the coated samples is rougher than the surface of the tempered sample. For the PB and BC-2 sample, in the first 15 min, the higher friction coefficients are attributed to the slightly rough surface, and the friction coefficient gradually decreases as the wear time increases. The BC-1 sample has the highest friction coefficient value. This may be because that the BC-1 sample has a large number of pores and cracks on the surface of the coating (see Figure 4b). Combining the wear morphologies, mass loss, and friction coefficients, the BC-2 sample is considered to have the best wear resistance. This is because the coating of the BC-2 sample contains a large amount of gradient-distributed, wear-resistant second phases (Cr_2B and Cr_xC_y), as discussed above.

3.5.3. Corrosion Resistance

Figure 10 displays the potentiodynamic polarisation curves of tempered and coated samples. Table 2 summarizes the parameters obtained through electrochemical tests, in which the corrosion rate (CR) is calculated by using the Faraday's equation [36]:

$$CR \text{ (mm/y)} = \frac{3.27 \times 10^{-3} \times I_{\text{corr}} \times EW}{\rho} \quad (2)$$

where I_{corr} is corrosion current density ($\mu\text{A}/\text{cm}^2$), EW is equivalent weight (28), and ρ is density ($7.85 \text{ g}/\text{cm}^3$). Clearly, the PB sample has a lower corrosion potential and higher corrosion current density than the tempered steel. Moreover, the corrosion rate obviously increases, indicating decrease in corrosion resistance after preboronizing treatment. This reduction in corrosion resistance may be caused by the presence of localized defects (such as pores and microcracks) in the coating [12,37]. The localized defects formed during preboronizing can act as a corrosion channel between the coating and the substrate, resulting in rapid corrosion of the coating and substrate. The corrosion resistance of both BC-1 and BC-2 samples is better than that of the as-tempered sample. Such improvement in corrosion resistance can be attributed to the formation of the Cr-rich layer (chromium carbides) and borides in the coating after chromizing treatment. It is well-known that both the chromium carbides and Cr have very strong passivity before breakdown at high potential [1], which leads to an increase in corrosion resistance. Additionally, it has been reported that the formation of borides (M_2B , such as Fe_2B and Cr_2B in this study) in the coatings can also improve the corrosion resistance [32].

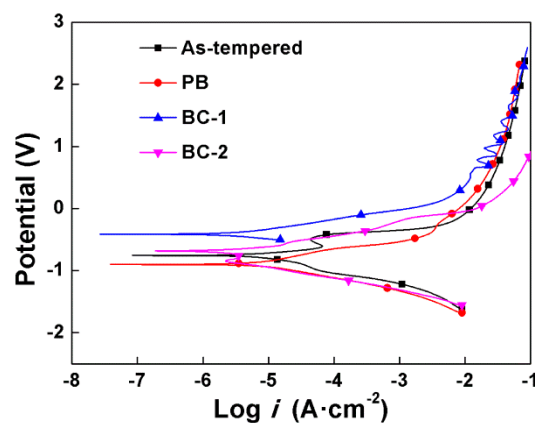


Figure 10. Potentiodynamic polarisation curves of various samples.

Table 2. Corrosion potential (E_{corr}), corrosion current density (I_{corr}), and average corrosion rate (Corr rate) of various samples.

Samples	E_{corr} (mV)	I_{corr} ($\mu\text{A}/\text{cm}^2$)	Corr Rate (mm/y)
As-tempered	-757	7.18	0.084
PB	-899	9.62	0.112
BC-1	-414	5.50	0.064
BC-2	-683	5.00	0.058

4. Conclusions

In this study, two-step duplex-alloyed coatings were prepared on the AISI 5140 steel by pack cementations. Microstructure and properties of the coating were characterized and studied. The main conclusions are as follows:

- After preboronizing at $950 \text{ }^\circ\text{C}$ for 3 h, a saw-toothed coating composed of columnar Fe_2B grains with an average thickness of about $69 \text{ }\mu\text{m}$ is formed.

- After chromizing at 1000 °C for 1 h, for the box-type furnace heating, the columnar F₂B grains do not completely decompose and are retained in the B-Cr coating, while for the induction heating, the F₂B grains disappear and are replaced by equiaxed grains of high-Cr pearlite embedded with block Cr₂B, block Cr_xC_y (Cr₂₃C₆ and Cr₇C₃), and a small amount of strip-like τ-phase Fe₂₃(C,B)₆ at the grain/phase boundaries.
- The efficiency of induction heating is higher than that of the box furnace heating, resulting in a thicker, denser, flatter surface, and a B-Cr coating with fully reacted B and Cr elements.
- For the thermal chromizing treatment, the subsurface decarburization is a common chronic disease. The preboronizing treatment can effectively solve the problem of subsurface decarburization.
- The wear resistance and corrosion resistance of the steel is significantly improved by the formation of B-Cr-rich coating.

Author Contributions: Conceptualization, J.H.; methodology, J.Z.; software, N.G.; validation, X.Y. and J.H.; formal analysis, Y.Y., J.H. and N.G.; investigation, J.H. and N.G.; resources, J.H.; data curation, J.H. and N.G.; writing—original draft preparation, J.H., J.Z. and N.G.; writing—review and editing, N.G.; supervision, N.G.; project administration, J.H., H.L. and N.G.; funding acquisition, J.H., H.L. and N.G.

Funding: This work was co-supported by the Natural Science Foundation of China (51575073 and 51501158), International Cooperation Special Project in Science and Technology of China (2015DFR70480), Scientific and Technological Research Program of Chongqing (cstc2017jcyjBX0031 and cstc2018jszx-cyzdX0125), Scientific and Technological Research Program of Banan District of Chongqing (2018TJ06), and Program for Innovation Team Building at Institutions of Higher Education in Chongqing (CXTDG20162017). N.G. special acknowledges the Fundamental Research Funds for the Central Universities of China (No. XDJK2019B066).

Conflicts of Interest: The authors declare no conflict of interest.

References

1. Hu, J.; Zhang, Y.; Yang, X.; Li, H.; Xu, H.; Ma, C.; Dong, Q.; Guo, N.; Yao, Z. Effect of pack-chromizing temperature on microstructure and performance of AISI 5140 steel with Cr-coatings. *Surf. Coat. Technol.* **2018**, *344*, 656–663. [[CrossRef](#)]
2. Hu, J.; Jiang, J.; Li, H.; Yang, X.; Xu, H.; Jin, Y.; Ma, C.; Dong, Q.; Guo, N. Effect of annealing treatment on microstructure and properties of Cr-coatings deposited on AISI 5140 Steel by brush-plating. *Coatings* **2018**, *8*, 193. [[CrossRef](#)]
3. Hu, J.; Ma, C.; Xu, H.; Guo, N.; Hou, T. Development of a composite technique for preconditioning of 41Cr4 steel used as gear material: examination of its microstructural characteristics and properties. *Sci. Technol. Nucl. Install.* **2016**, *2016*, 1–6. [[CrossRef](#)]
4. Hu, J.; Ma, C.; Yang, X.; Xu, H.; Guo, N.; Yu, H. Microstructure evolution during continuous cooling in AISI 5140 steel processed by induction heating chromizing. *J. Mater. Eng. Perform.* **2017**, *26*, 5530–5537. [[CrossRef](#)]
5. Li, X.; Liu, S.; Wang, J.; Yu, M.; Tang, H. Effect of different ZrN addition on microstructure and wear properties of titanium based coatings by laser cladding technique. *Coatings* **2019**, *9*, 261. [[CrossRef](#)]
6. Iorga, S.; Ciuca, S.; Leuvrey, C.; Colis, S. Influence of the thermo-chemical conditions on the carbo-chromization process of α-Fe matrices obtained by powder sintering technique. *J. Alloy. Compd.* **2012**, *512*, 100–104. [[CrossRef](#)]
7. Fesahat, M.; Soltanieh, M.; Eivani, A.R. Effect of plasma nitriding on nanostructure of TRD coating. *Surf. Eng.* **2016**, *32*, 547–553. [[CrossRef](#)]
8. Biesuz, M.; Sglavo, V.M. Chromium and vanadium carbide and nitride coatings obtained by TRD techniques on UNI 42CrMoS4 (AISI 4140) steel. *Surf. Coat. Technol.* **2016**, *286*, 319–326. [[CrossRef](#)]
9. Zeng, D.; Yang, S.; Xiang, Z.D. Formation of hard surface layer on austenitic stainless steels via simultaneous chromising and nitriding by pack cementation process. *Appl. Surf. Sci.* **2012**, *258*, 5175–5178. [[CrossRef](#)]
10. Adachi, S.; Ueda, N. Wear and corrosion properties of cold-sprayed AISI 316L coatings treated by combined plasma carburizing and nitriding at low temperature. *Coatings* **2018**, *8*, 456. [[CrossRef](#)]
11. Balusamy, T.; Narayanan, T.S.; Ravichandran, K. Effect of surface mechanical attrition treatment (SMAT) on boronizing of EN8 steel. *Surf. Coat. Technol.* **2012**, *213*, 221–228. [[CrossRef](#)]
12. Aghaie-Khafri, M.; Abady, M.M.N. A study of chromo-boronizing on DIN 1.2714 steel by duplex surface treatment. *JOM-US* **2012**, *64*, 694–701. [[CrossRef](#)]

13. Balusamy, T.; Narayanan, T.S.; Ravichandran, K.; Park, I.S.; Lee, M.H. Pack boronizing of AISI H11 tool steel: Role of surface mechanical attrition treatment. *Vacuum* **2013**, *97*, 36–43. [[CrossRef](#)]
14. Joshi, A.A.; Hosmani, S.S.; Dumbre, J. Tribological performance of boronized, nitrided, and normalized AISI 4140 steel against hydrogenated diamond-like carbon-coated AISI D2 steel. *Tribol. Trans.* **2015**, *58*, 500–510. [[CrossRef](#)]
15. Lentz, J.; Röttger, A.; Theisen, W. Solidification and phase formation of alloys in the hypoeutectic region of the Fe–C–B system. *Acta Mater.* **2015**, *99*, 119–129. [[CrossRef](#)]
16. Khalaj, G.; Nazari, A.; Khoie, S.M.M.; Khalaj, M.J.; Pouraliakbar, H. Chromium carbonitride coating produced on DIN 1.2210 steel by thermo-reactive deposition technique: thermodynamics, kinetics and modeling. *Surf. Coat. Technol.* **2013**, *225*, 1–10. [[CrossRef](#)]
17. Kurt, B.; Küçük, Y.; Sabri Gök, M. Microabrasion wear behavior of VC and CrC coatings deposited by thermoreactive diffusion technique. *Tribol. Trans.* **2014**, *57*, 345–352. [[CrossRef](#)]
18. Mahdavi, A.; Medvedovski, E.; Mendoza, G.; McDonald, A. Corrosion resistance of boronized, aluminized, and chromized thermal diffusion-coated steels in simulated high-temperature recovery boiler conditions. *Coatings* **2018**, *8*, 257. [[CrossRef](#)]
19. Zandrahimi, M.; Vatandoost, J.; Ebrahimifar, H. Pack cementation coatings for high-temperature oxidation resistance of AISI 304 stainless steel. *J. Mater. Eng. Perform.* **2012**, *21*, 2074–2079. [[CrossRef](#)]
20. Petrova, R.S.; Suwattananont, N.; Samardzic, V. The effect of boronizing on metallic alloys for automotive applications. *J. Mater. Eng. Perform.* **2008**, *17*, 340–345. [[CrossRef](#)]
21. Ozbek, I.; Bindal, C. Kinetics of borided AISI M2 high speed steel. *Vacuum* **2011**, *86*, 391–397. [[CrossRef](#)]
22. Samadi, V.; Habibolahzade, A. Evaluation of microstructures and wear properties of duplex boride coatings. *Mater. Sci. Technol.* **2013**, *26*, 41–46. [[CrossRef](#)]
23. Wang, X.; Zhang, R.; Zhou, T.; Wei, X.; Liaw, P.; Feng, R.; Wang, W.; Li, R. Microstructural evolution in chroming coatings friction pairs under dry sliding test conditions. *Adv. Tribol.* **2018**, *2018*, 1–6. [[CrossRef](#)]
24. Kheyrodin, M.; Habibolahzadeh, A.; Mousavi, S.Y.B. Wear and corrosion behaviors of duplex surface treated 316L austenitic stainless steel via combination of boriding and chromizing. *Prot. Met. Phys. Chem. Surf.* **2017**, *53*, 105–111. [[CrossRef](#)]
25. Tabur, M.; Izciler, M.; Gul, F.; Karacan, I. Abrasive wear behaviour of boronized AISI8620 steel. *Wear* **2009**, *266*, 1106–1112. [[CrossRef](#)]
26. Lentz, J.; Röttger, A.; Theisen, W. Mechanism of the Fe₃(B,C) and Fe₂₃(C,B)₆ solid-state transformation in the hypoeutectic region of the Fe–C–B system. *Acta Mater.* **2016**, *119*, 80–91. [[CrossRef](#)]
27. Kartal, G.; Eryilmaz, O.L.; Krumdick, G.; Erdemir, A.; Timur, S. Kinetics of electrochemical boriding of low carbon steel. *Appl. Surf. Sci.* **2011**, *257*, 6928–6934. [[CrossRef](#)]
28. Lackner, J.; Waldhauser, W.; Major, L.; Kot, M. Tribology and micromechanics of chromium nitride based multilayer coatings on soft and hard substrates. *Coatings* **2014**, *4*, 121–138. [[CrossRef](#)]
29. Guo, N.; Liu, Q.; Xin, Y.; Luan, B.; Zhou, Z. The application of back-scattered electron imaging for characterization of pearlitic steels. *Sci. China Technol. Sci.* **2011**, *54*, 2368–2372. [[CrossRef](#)]
30. Ma, S.; Xing, J.; Fu, H.; Gao, Y.; Zhang, J. Microstructure and crystallography of borides and secondary precipitation in 18 wt.% Cr–4 wt.% Ni–1 wt.% Mo–3.5 wt.% B–0.27 wt.% C steel. *Acta Mater.* **2012**, *60*, 831–843. [[CrossRef](#)]
31. Joshi, A.A.; Hosmani, S.S. Pack-boronizing of AISI 4140 steel: Boronizing mechanism and the role of container design. *Mater. Manuf. Process.* **2014**, *29*, 1062–1072. [[CrossRef](#)]
32. Zhang, C.; Chen, G.J.; Dai, P.Q. Evolution of the microstructure and properties of laser-clad FeCrNiCoB_x high-entropy alloy coatings. *Mater. Sci. Technol.* **2016**, *32*, 1666–1672. [[CrossRef](#)]
33. Hosmani, S.S.; Kuppusami, P.; Goyal, R.K. Chromizing, carburizing, and duplex surface treatment. In *An Introduction to Surface Alloying of Metals*; Springer: New Delhi, India, 2014; pp. 89–101.
34. Praveen, A.S.; Arjunan, A. Parametric optimisation of high-velocity oxy-fuel nickel-chromium-silicon- boron and aluminium-oxide coating to improve erosion wear resistance. *Mater. Res. Express* **2019**, *6*, 096560. [[CrossRef](#)]
35. Priyan, M.S. Wear and corrosion studies of Fe–B–Cr alloy coating on en 24 steel by HVOF thermal spray method. *Surf. Eng. Appl. Electrochem.* **2017**, *53*, 580–586. [[CrossRef](#)]

36. Khara, S.; Choudhary, S.; Sangal, S.; Mondal, K. Corrosion resistant Cr-coating on mild steel by powder roll bonding. *Surf. Coat. Technol.* **2016**, *296*, 203–210. [[CrossRef](#)]
37. Kayali, Y.; Büyüksağış, A.; Yalçın, Y. Corrosion and wear behaviors of boronized AISI 316L stainless steel. *Met. Mater. Int.* **2013**, *19*, 1053–1061. [[CrossRef](#)]



© 2019 by the authors. Licensee MDPI, Basel, Switzerland. This article is an open access article distributed under the terms and conditions of the Creative Commons Attribution (CC BY) license (<http://creativecommons.org/licenses/by/4.0/>).